InGaAs x-ray photodiode for spectroscopy

Article (Published Version)

Materials Research Express

PAPER • **OPEN ACCESS**

InGaAs x-ray photodiode for spectroscopy

To cite this article: M D C Whitaker *et al* 2020 *Mater. Res. Express* **7** 105901

Materials Research Express

PAPER

InGaAs x-ray photodiode for spectroscopy

M D C Whitaker[1], G Lioliou[1], A B Krysa[2] and A M Barnett[1]

[1] Space Research Group, Sch. of Mathematical and Physical Sciences, University of Sussex, Falmer, Brighton, BN1 9QT, United Kingdom
[2] EPSRC National Epitaxy Facility, Dept of Electrical and Electronic Engineering, University of Sheffield, Mappin Street, Sheffield, S1 3JD, United Kingdom

E-mail: M.Whitaker@sussex.ac.uk

Keywords: InGaAs, GaInAs, x-ray detector, Photodiode, Spectroscopy

OPEN ACCESS

RECEIVED
23 July 2020

REVISED
14 September 2020

ACCEPTED FOR PUBLICATION
23 September 2020

PUBLISHED
7 October 2020

Abstract

A prototype $In_{0.53}Ga_{0.47}As$ p^+-i-n^+ x-ray photodiode, fabricated from material grown by metalorganic vapour phase epitaxy, was investigated as a novel detector of x-rays. The detector was connected to a custom low-noise charge sensitive preamplifier and standard readout electronics to produce an x-ray spectrometer. The detector and preamplifier were operated at a temperature of 233 K (−40 °C). An energy resolution of 1.18 keV ± 0.06 keV Full Width at Half Maximum at 5.9 keV was achieved. This is the first time InGaAs (GaInAs) has been shown to be capable of spectroscopic photon counting x-ray detection.

The compound semiconductor $In_xGa_{1-x}As$ has found utility across a wide number of applications; including, but not limited to, laser diodes [1–3], single photon avalanche detectors [4, 5], eye-safe 3D laser scanning (Lidar) [6–8], and transistors [9, 10]. However, to date, there has been no report of the suitability of $In_xGa_{1-x}As$ photodiodes as detectors for x-ray (or γ-ray) photon counting spectroscopy.

At present, in environments where low temperature (< 300 K) operation is possible, Ge (bandgap, $E_g = 0.66$ eV at 300 K [11]) and Si ($E_g = 1.12$ at 300 K [12]) x-ray detectors are commonplace [13]. Detectors of both materials can provide good Fano-limited energy resolutions (101 eV [14] and 120 eV [15] full width at half maximum, *FWHM*, at 5.9 keV), but Ge has better (larger) linear x-ray absorption coefficients (841 cm^{-1} cf 356 cm^{-1} at 5.9 keV [16]). Consideration of alternative detector materials, with possibly even better properties, is also interesting. In this letter, an $In_{0.53}Ga_{0.47}As$ ($E_g = 0.75$ eV at 300 K [17]) photodiode is demonstrated to be capable of spectroscopic x-ray detection for the first time. The immediate attraction of the material is that its linear x-ray absorption coefficients are better than those of both Ge and Si (e.g. 1530 cm^{-1} for $In_{0.53}Ga_{0.47}As$ at 5.9 keV [16]). Another favourable indication for $In_{0.53}Ga_{0.47}As$ is that devices made from the material have been reported with very small leakage currents ($\approx 10^{-14}$ A) [18]; this is important because leakage currents in part control the parallel white noise of x-ray spectrometers and therefore play a key role in setting the energy resolution achievable in such spectrometers [19].

An $In_{0.53}Ga_{0.47}As$ p^+-i-n^+ structure (see table 1) was grown by metalorganic vapour phase epitaxy on an (100) InP n^+ substrate. Circular mesa photodiodes (200 μm diameter) were fabricated by a two-step wet etching in 1:1:1 HBr:$K_2Cr_2O_7$:CH_3CO_2H and 1:8:80 H_2SO_4:H_2O_2:H_2O solutions. A quasi-annular top metal contact (200 nm Au, 20 nm Ti; covering 45% of the diode's face) was evaporated onto the p^+ side of each mesa structure. A rear planar metal contact (200 nm Au, 20 nm InGe) was evaporated onto the rear of the substrate. A randomly selected photodiode was packaged in a TO-5 can and gold ball-wedge wirebonded.

The packaged detector was connected to a custom-made feedback resistorless charge-sensitive preamplifier (similar to [20]) and standard onwards readout electronics as per [21]. The detector and preamplifier were installed within a TAS Micro MT environmental chamber, which was continually purged with dry N_2 [22]. An ^{55}Fe radioisotope x-ray (Mn Kα = 5.9 keV; Mn Kβ = 6.49 keV) source (activity $\approx$ 164 MBq) was placed atop the $In_{0.53}Ga_{0.47}As$ x-ray photodiode with $\approx$ 4 mm between the source and photodiode. A thermocouple was positioned appropriately in order to monitor the temperature of the detector and preamplifier. The internal temperature of the environmental chamber was reduced to 233 K (−40 °C). The remaining electronics chain

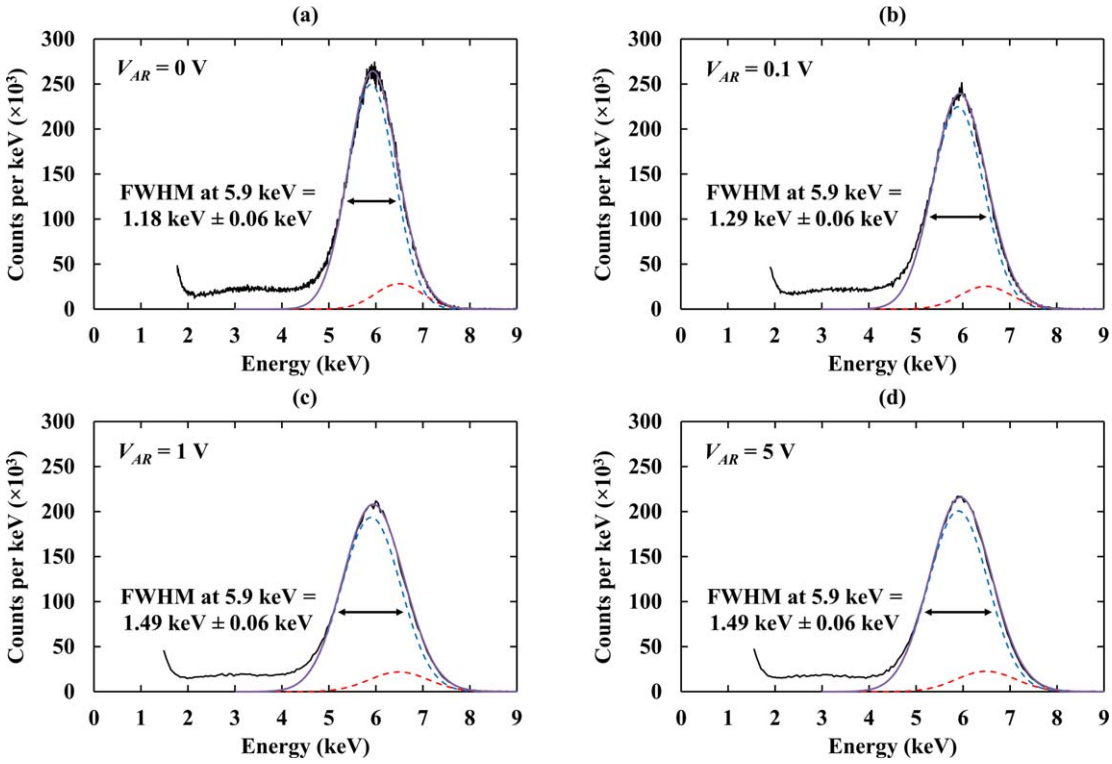

Figure 1. ^{55}Fe x-ray spectra accumulated with the $In_{0.53}Ga_{0.47}As$ p^+-i-n^+ x-ray photodiode based spectrometer operated at a temperature of 233 K (−40 °C) and a shaping time of 0.5 μs, with the detector at applied reverse biases, V_{AR}, of: (a) 0 V; (b) 0.1 V; (c) 1 V; and (d) 5 V (black lines). The fitted peaks of Mn Kα (5.9 keV, blue dashed lines) and Mn Kβ (6.49 keV, red dashed lines), together with the combination of those peaks (purple solid lines), are also shown. The Mn Kα and Mn Kβ peaks were not resolved individually and so form a combined peak in the detected spectra. The spectra were normalised into counts per keV in order to account for the differing multi-channel analyser channel widths of each spectrum.

Table 1. Layer details of the $In_{0.53}Ga_{0.47}As$ p^+-i-n^+ structure from which the device was fabricated.

Material	Dopant	Dopant type	Thickness (nm)	Doping density (cm^{-3})
InP	Zn	p^+	10	1×10^{19}
$In_{0.53}Ga_{0.47}As$	Zn	p^+	200	2×10^{18}
$In_{0.53}Ga_{0.47}As$			5000	Undoped
$In_{0.53}Ga_{0.47}As$	Si	n^+	100	2×10^{18}
InP	Si	n^+	200	2×10^{18}
InP n^+ substrate	Si			

was kept at room temperature. Once the detector, preamplifier, and chamber atmosphere had reached thermal equilibrium at 233 K, measurements were started.

^{55}Fe x-ray spectra were acquired with the $In_{0.53}Ga_{0.47}As$ x-ray photodiode operated at applied reverse biases, V_{AR}, of 0 V, 0.1 V, 1 V, and 5 V; the spectra accumulated can be seen in figure 1. A shaping time, τ, of 0.5 μs (the shortest available on the Ortec 572 A shaping amplifier and that which gave the best energy resolution of those available) and a live time limit of 200 s were set for each accumulation. A defined photopeak, the combination of the detected Mn Kα (5.9 keV) and Mn Kβ (6.49 keV) x-rays emitted from the ^{55}Fe radioisotope x-ray source, was detected at all investigated applied biases, as shown in figure 1. Since: (a) the emission characteristics of ^{55}Fe were well known [23] and the details of the material's encapsulation into the laboratory source were understood; (b) the x-ray linear absorption and attenuation coefficients of $In_{0.53}Ga_{0.47}As$ were readily calculable [24]; and (c) the detector's structure was known *a priori*, it was possible to deconvolve the detected peak into the respective Mn Kα and Mn Kβ contributions in order to establish the *FWHM* at 5.9 keV. To do this, two Gaussians (one each for the Mn Kα and Mn Kβ contributions respectively, and taking into account the considerations above) were computed, where the summation of the two Gaussians fitted the measured photopeak. In each spectrum, the peak centre of the single detected photopeak, which was the combination of the unresolved Mn Kα and Mn Kβ photopeaks, was 5.94 keV $\pm$ 0.02 keV. The measured *FWHM* of the Mn Kα (5.9 keV) peak (*FWHM* at 5.9 keV) increased (degraded) as a function of increased applied detector reverse bias, from 1.18 keV $\pm$ 0.06 keV at 0 V to

Table 2. Measured leakage current, capacitance, and depletion width of the $In_{0.53}Ga_{0.47}As$ p^+-i-n^+ x-ray photodiode at 233 K (−40 °C).

Applied reverse bias (V)	Detector current (pA)	Detector capacitance (pF)	Depletion width (μm)
0	4.9 ± 0.4	1.77 ± 0.02	2.19 ± 0.04
1	255 ± 1	1.43 ± 0.02	2.70 ± 0.04
2	344 ± 1	1.38 ± 0.02	2.81 ± 0.04
3	391 ± 2	1.32 ± 0.02	2.88 ± 0.04
4	420 ± 2	1.26 ± 0.02	2.95 ± 0.04
5	441 ± 2	1.09 ± 0.02	3.07 ± 0.04

1.49 keV ± 0.06 keV at 5 V. Detector self-fluorescence of the In L shell ($L\alpha_1 = 3.29$ keV, $L\alpha_2 = 3.28$ keV, $L\beta_1 = 3.49$ keV, $L\beta_2 = 3.71$ keV, $L\gamma_1 = 3.92$ keV) caused the increased number of counts apparent in the spectra around those energies. Partial collection of charge created in the non-active regions of the detector gave rise to the rest of the low energy tailing [25]. Whilst most of the zero energy noise peak was eliminated by setting a low energy discriminator threshold after establishing the zero energy peak's position on the multi-channel analyser, a small portion of it can still be seen in each spectrum.

The leakage current and capacitance of the detector itself (i.e. with packaging effects subtracted) were measured at the same temperature at which spectra were accumulated using a Keithley 6487 picoammeter and an HP 4275 A LCR meter (1 MHz frequency; 50 mV rms signal magnitude), respectively. The results are summarised in table 2, along with the implied depletion width of the detector (calculated assuming a parallel plate capacitance [22]). The package itself contributed an additional 0.79 pF ± 0.01 pF of capacitance. The package leakage current was found to be negligible (⩽0.02 pA) and fell well within the measurement uncertainty (± 0.4 pA) of the total leakage current. The calculated depletion widths and the impact ionisation coefficients of $In_{0.53}Ga_{0.47}As$ [26] indicated that the detector was operating in non-avalanche mode across the reverse bias range employed.

The energy resolution (*FWHM*) of a non-avalanche semiconductor photodiode x-ray spectrometer is given by

$$FWHM\ [\mathrm{eV}] = \omega\left(\frac{8\ln(2)FE}{\omega} + R^2 + A^2\right)^{0.5}, \quad (1)$$

where ω is the electron-hole pair creation energy, F is the Fano factor of the material, E is the incident photon energy, R is the total electronic noise of the spectrometer (the quadratic sum of all series white, parallel white, $1/f$, dielectric, and induced gate drain current noises), and A is any incomplete charge collection noise arising from the detector. When R and A are zero, equation (1) reduces to the Fano limit of the energy resolution for a given material. Whilst F and ω have yet to be measured and reported for $In_{0.53}Ga_{0.47}As$, it is informative to make cautious estimations of these parameters in the context of considering the noise sources contributing to the overall achieved energy resolutions reported in figure 1.

Considering the ternary nature of the detector material and the high atomic numbers of its constituent elements, the Fano factor of $In_{0.53}Ga_{0.47}As$ is likely to be larger than those of Si and Ge; thus a highly cautious value of 0.14 is assumed for the purposes of the estimation. The relationship between E_g and ω is still a topic of investigation [27], but for present purposes, an estimate of $\omega = 3.05$ eV ± 0.13 eV may be made for $In_{0.53}Ga_{0.47}As$ at 300 K, given $E_g = 0.75$ eV at 300 K [17] and use of the Bertuccio-Maiocchi-Barnett (BMB) relationship [27]. Thus a Fano limit of 118 eV ± 6 eV *FWHM* at 5.9 keV may be estimated for $In_{0.53}Ga_{0.47}As$ at 300 K which is comparable to those of Ge and Si.

Given the leakage current and capacitance of the detector and its packaging, and a priori knowledge of the custom preamplifier, approximations of at least some of the white parallel, white series (including induced gate drain current noise), $1/f$, and dielectric noise contributions from the preamplifier and the detector itself, could be calculated as per [28–30]. The calculated white parallel noise included the leakage current associated with the detector, the detector packaging, and the gate leakage current of the input JFET which was estimated to be 1 pA [31]. The calculated white series noise included the capacitance associated with the detector, the detector packaging, and the input JFET capacitance which was estimated to be 2 pF [31]. The calculated dielectric noise included the detector dielectric contribution (assuming a dielectric dissipation factor of 0.001 for $In_{0.53}Ga_{0.47}As$), the detector packaging dielectric contribution (assuming a dielectric dissipation factor of 0.01), and the input JFET dielectric contribution (assuming a dielectric dissipation factor of 0.0008 [32]). Figure 2 presents those calculated noise contributions, as well as the estimated Fano limit (118 eV ± 6 eV at 5.9 keV at 300 K). Although the temperature dependence of ω and F for $In_{0.53}Ga_{0.47}As$ are unknown at present, the

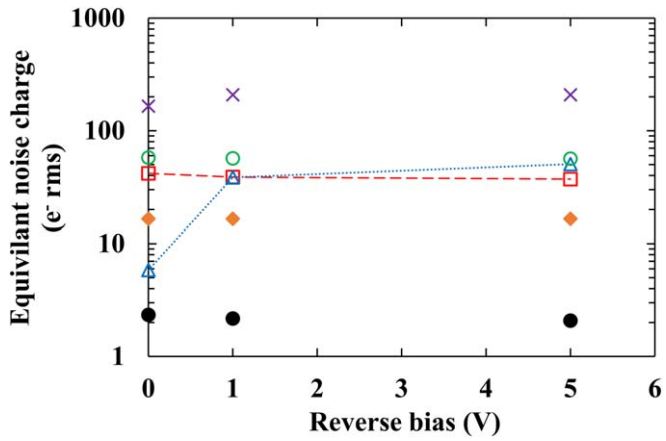

Figure 2. Measured energy resolution in equivalent noise charge (purple × symbols) as a function of applied detector reverse bias, at a shaping time of 0.5 μs and with the system operated at a temperature of 233 K (−40 °C). The calculated dielectric noise (green empty circles), calculated series white noise including induced gate drain current noise (red empty squares), estimated Fano noise (orange filled diamonds), calculated parallel white noise (blue empty triangles), and calculated $1/f$ noise (black filled circles) are also plotted. The dashed and dotted lines are guides for the eyes only.

difference in the Fano-limited energy resolution between 300 K and 233 K is unlikely to be significant compared with the large non-Fano noises present in the reported system.

The degradation in energy resolution (*FWHM* at 5.9 keV) of the spectrometer as a function of increased applied detector reverse bias (1.18 keV ± 0.06 keV at 0 V cf 1.49 keV ± 0.06 keV at 5 V) was explained, in part, by the increase in calculated parallel white noise (contributing 41 eV ± 3 eV at 0 V cf 360 eV ± 2 eV at 5 V). However, it should be noted that the values calculated for the various noise components when combined in quadrature with the likely Fano noise did not amount to the entirety of the noise observed to be present in the system; the remaining noise contribution, calculated by subtracting in quadrature the calculated noise contributions (including the estimated Fano limit) from the measured energy resolution, remained significant, increasing from a contribution of 1.06 keV ± 0.07 keV at 0 V to 1.36 keV ± 0.07 keV at 5 V. This remaining noise contribution included additional stray electronic noises, which remained unaccounted in the approximation employed to estimate the electronic noise contributions, likely originating from lossy dielectrics in proximity to the gate of the input JFET, as well as parasitic components of white parallel and stray white series noise arising within the system; incomplete charge collection noise may also have played a part.

Since the depletion width of the $In_{0.53}Ga_{0.47}As$ x-ray photodiode did not extend across the 5 μm i layer (see table 2) within the investigated applied reverse bias range, incomplete charge collection noise may have been present, particularly from the non-depleted region of the i layer, but this cannot be quantified from the present results. In addition, the large leakage current of the $In_{0.53}Ga_{0.47}As$ detector (e.g. 441 pA ± 5 pA at 5 V applied reverse bias) may have adjusted the operating bias condition of the preamplifier input JFET, which is in part set by the leakage current of the detector in feedback resistorless designs such as the one used here [20]; this may have increased the leakage current and consequently the parallel white noise contribution of the JFET. Although the JFET leakage current was estimated to be 1 pA at the optimal operating bias condition (equivalent to 17 eV parallel white noise), this can increase to >10 nA when it is operated in suboptimal bias conditions (equivalent to >1.71 keV parallel white noise) [31]. The increase in noise brought by modification of the bias point of the JFET was included in the quantity of noise classified as stray, and likely explains, in part, the variation of the stay noise contribution with detector bias.

In summary, InGaAs has been shown to be capable of photon counting x-ray spectroscopy for the first time. An energy resolution of 1.18 keV ± 0.06 keV *FWHM* at 5.9 keV at a temperature of 233 K (−40 °C) was achieved using a prototype $In_{0.53}Ga_{0.47}As$ p^+-i-n^+ photodiode coupled to a charge-sensitive preamplifier and standard onwards readout electronics. Although the energy resolution achieved was modest compared to current gold-standard cooled spectrometers using Ge or Si detectors, as well as other uncooled prototype detectors such as AlGaAs (630 eV *FWHM* at 5.9 keV at 20 °C [27]), CdZnTe (270 eV *FWHM* at 5.9 keV at room temperature [33]), GaAs (250 eV *FWHM* at 5.9 keV at −5 °C [34]), and InGaP (770 eV FWHM at 5.9 keV at 20 °C [35]), further development of InGaAs x-ray detectors is likely to improve the performance attainable. In addition, recent work on superlattice structures [36–38] may help to improve the *FWHM* of future InGaAs x-ray detector designs. This promise, together with the results already obtained, as well as the large x-ray absorption coefficients of InGaAs and the possibility of developing spectroscopic $In_{0.53}Ga_{0.47}As$-InP hetrojunction x-ray avalanche photodiodes, provides motivation for further work on x-ray detectors made from the material in

future. In order to inform future development of InGaAs x-ray spectrometers, investigation of their performance as a function of temperature and in response to illumination with different energy x-rays and γ-rays (e.g. those from ^{241}Am and ^{109}Cd radioisotope x-ray/γ-ray sources) would be valuable.

Acknowledgments

This work was supported, in part, by the Science and Technology Facilities Council, UK; Grants ST/P001815/1 and ST/R001804/1 A M B acknowledges funding from the Leverhulme Trust, UK, in the form of a 2016 Philip Leverhulme Prize. The authors are grateful to R J Airey and S. Kumar at University of Sheffield for device fabrication.

Authors' data statement

All data that support the findings of this study are included within the article (and any supplementary information files).

ORCID iDs

M D C Whitaker https://orcid.org/0000-0001-6109-5793
G Lioliou https://orcid.org/0000-0002-6989-7106
A B Krysa https://orcid.org/0000-0001-8320-7354

References

[1] Gessner R, Drumski M and Beschorner M 1989 *Electron. Lett.* **25** 516
[2] Krysa A B, Roberts J S, Green R P, Wilson L R, Page H, Garcia M and Cockburn J W 2004 *J. Cryst. Growth* **272** 682
[3] Ajili L, Scalari G, Hoyler N, Giovannini M and Faist J 2005 *Appl. Phys. Lett.* **87** 141107
[4] Pellegrini S, Warburton R E, Tan L J J, Ng J S, Krysa A B, Groom K, David J P R, Cova S, Robertson M J and Buller G S 2006 *IEEE J. Quantum Electron.* **42** 397
[5] Buller G S, Warburton R E, Pellegrini S, Ng J S, David J P R, Tan L J J, Krysa A B and Cova S 2007 *IET Optoelectron.* **1** 249
[6] Pawlikowska A M, Halimi A, Lamb R A and Buller G S 2017 *Opt. Express* **25** 11919
[7] Gong W, Chyba T H and Temple D A 2007 *Opt. Lasers Eng.* **45** 898
[8] Liang Y, Fei Q, Liu Z, Huang K and Zeng H 2019 *Photonics Research* **7** 1
[9] del Alamo J A, Antoniadis D, Guo A, Kim D H, Kim T W, Lin J, Lu W, Vardi A and Zhao X 2013 *InGaAs MOSFETs for CMOS: Recent advances in process technology IEEE Int. Electron Devices Meeting, Washington, DC, USA*
[10] Maleeva N A *et al* 2019 *Tech. Phys. Lett.* **45** 1092
[11] Sze S M 2006 *Physics of Semiconductor Devices* (New Jersey: Wiley) 3rd ed
[12] Bludau W, Onton A and Heinke W 1974 *J. Appl. Phys.* **45** 1846
[13] Lowe B G and Sareen R A 2014 *Semiconductor X ray Detectors* (Florida: Taylor & Francis Group)
[14] Lowe B G 1997 *Nucl. Instrum. Methods Phys. Res., Sect. A* **399** 354
[15] Lowe B G and Sareen R A 2007 *Nucl. Instrum. Methods Phys. Res., Sect. A* **576** 367
[16] Hubbell J H 1982 *Int. J. Appl. Radiat. Isot.* **33** 1269
[17] Takeda Y, Sasaki A, Imamura Y and Takagi T 1976 *J. Appl. Phys.* **47** 5405
[18] Mizumoto I and Mashiko S 1993 *Electron. Lett.* **29** 234
[19] Lioliou G and Barnett A M 2015 *Nucl. Instrum. Methods Phys. Res., Sect. A* **801** 63
[20] Bertuccio G, Rehak P and Xi D 1993 *Nucl. Instrum. Methods Phys. Res., Sect. A* **326** 71
[21] Lioliou G, Poyser C L, Butera S, Campion R P, Kent A J and Barnett A M 2019 *Nucl. Instrum. Methods Phys. Res., Sect. A* **946** 162670
[22] Whitaker M D C, Lioliou G and Barnett A M 2018 *Nucl. Instrum. Methods Phys. Res., Sect. A* **899** 106
[23] Schötzig U 2000 *Appl. Radiat. Isot.* **53** 469
[24] Cromer D T and Liberman D 1970 *J. Chem. Phys.* **53** 1891
[25] Barnett A M, Lioliou G and Ng J S 2015 *Nucl. Instrum. Methods Phys. Res., Sect. A* **774** 29
[26] Ng J S, Tan C H, David J P R, Hill G and Rees G J 2003 *IEEE Trans. Electron Devices* **50** 901
[27] Whitaker M D C, Lioliou G, Krysa A B and Barnett A M 2020 *Semicond. Sci. Technol.* **35** 9
[28] Bertuccio G, Pullia A and De G 1996 *Geronimo, Nucl. Instrum. Methods Phys. Res., Sect. A* **380** 301
[29] Gatti E, Manfredi P F, Sampietro M and Speziali V 1990 *Nucl. Instrum. Methods Phys. Res., Sect. A* **297** 467
[30] Barnett A M, Lees J E, Bassford D J and Ng J S 2012 *Nucl. Instrum. Methods Phys. Res., Sect. A* **673** 10
[31] Siliconix 2001 2N4416/2N4416A/SST4416 N-Channel JFETs, S52424, Rev. E, Vishay Electronic GmbH, Selb
[32] Bertuccio G and Casiraghi R 2003 *IEEE Trans. Nucl. Sci.* **50** 1
[33] Owens A, Buslaps T, Erd C, Graafsma H, Lumb D and Welter E 2006 *Nucl. Instrum. Methods Phys. Res., Sect. A* **563** 268
[34] Erd C, Owens A, Brammertz G, Bavdaz M, Peacock A, Lamsa V, Nenonen S, Andersson H and Haack N 2002 *Nucl. Instrum. Methods Phys. Res., Sect. A* **487** 78
[35] Butera S, Lioliou G, Krysa A B and Barnett A M 2018 *Nucl. Instrum. Methods Phys. Res., Sect. A* **908** 277
[36] Chang Y, Grein C H, Becker C R, Huang J, Ghosh S, Aqariden F and Sivananthan S 2011 *J. Electron. Mater.* **40** 1854
[37] Shi Y, Zhang Y, Ma Y, Gu Y, Chen X, Gong Q, Du B, Zhang J and Zhu Y 2018 *Infrared Phys. Technol.* **89** 72
[38] Suzuki A, Yamada A, Yokotsuka T, Idota K and Ohki Y 2002 *Japan. J. Appl. Phys.* **41** 1182